Equivalent Circuits for Nonsymmetric Reciprocal Two Ports Based on Eigenstate Formulation

Elena Abdo-Sánchez, *Member, IEEE*, Carlos Camacho-Peñalosa, *Senior Member, IEEE*, Teresa M. Martín-Guerrero, and Jaime Esteban

***Abstract*— Equivalent circuit topologies for two-port reciprocal nonsymmetric structures are proposed as an extension of the well-known symmetric lattice network. An eigenstate formulation approach that allows the separation of the eigenmodes in the equivalent circuit, as in the symmetric lattice network, is adopted. Four topologies based on series or parallel immittances with the combined use of some transformers are proposed. Particular cases, such as symmetric networks and parallel and series single elements, are derived from the proposed topologies. Moreover, power dissipation in these topologies is also analyzed. A modification in the reference planes is further introduced to achieve power dissipation orthogonality in the two branches of the circuit, as happens in the symmetric lattice network. Additionally, real transformation ratios for the transformers and nonnegative real parts for the immittances are obtained. Finally, the equivalent circuit is extracted for a complementary strip slot with different degrees of asymmetry. This illustrative example confirms the usefulness of the proposed topologies, which can be regarded as an extension of the symmetric lattice network, since they preserve the eigenstate decomposition.**

***Index Terms*— Asymmetry, eigenstates, eigenvectors, equivalent circuit, lattice network.**

I. Introduction

ALTHOUGH the use of the lattice network [1] for circuit modeling was proposed many years ago, its use has not been as widespread as other topologies like the T- or Π-networks. However, its application has been lately encouraged in several fields, like artificial transmission lines [2]–[4] or the modeling of coupled transmission lines [5]. The important advantages of this network are that it guarantees realizability of its elements [6, Sec. 4.7] and it allows the separation of the even- and odd-mode excitations in the equivalent circuit, as stated in Bartlett's theorem [7]. Both features have been already exploited by the authors: 1) to propose the lattice network for the modeling of transmission line symmetric components and discontinuities [8] and 2) to be able to use the even/odd mode power dissipation independence for the radiation analysis of certain symmetric structures [9].

Recently, the lattice network was proposed for the general modeling of the unit cell of leaky-wave antennas scanning through broadside [10]. In an attempt to generalize the formulation of [10] to asymmetric unit cells, Otto *et al.* [11] proposed an asymmetric circuit network that accounts for the asymmetry by means of some transformers. They derived this circuit from a representation of the symmetric lattice network by including four ideal transformers. Although it is clear that the asymmetric proposed network leads to the symmetric lattice network in the symmetric case, no additional explanation is provided for the derivation of this generalized lattice network. Moreover, the transformation ratios of the transformers are eventually assumed to be real, when in the mathematical formulation they are complex numbers.

In order to avoid the problems (concerning passivity and stability) of the pole-residue expansions applied to cast Y- or Z-parameters in a Π- or T-network, the network synthesis of symmetric structures based on an eigenstate formulation (even- and odd-mode contributions) was proposed in [12]. The equivalent circuit topology that allows this eigenstate-based modeling is, indeed, the symmetric lattice network.

In this contribution, the eigenstate formulation approach of [12] is adopted to propose general equivalent circuits for asymmetric reciprocal structures, considering the general lossy case. In fact, this derivation can be regarded as an extension of the symmetric lattice network for asymmetric structures. Unlike the work and topology in [11], the proposed topologies preserve the property of symmetric lattice networks of being decomposable in eigenstates. Moreover, power dissipation orthogonality between the two branches of the circuit is also achieved, thus successfully extending this property of symmetric lattice networks [9] to asymmetric topologies. Additionally, it is demonstrated how the circuit can be modified to achieve real transformation ratios for the transformers and nonnegative real parts for the resulting immittances, as desired for proper modeling.

This paper is structured as follows. Section II contains the derivation of the proposed equivalent circuits, derives the symmetric lattice network as a particular case of the proposed topologies, and analyzes the special cases of a single

Manuscript received April 21, 2017; accepted May 10, 2017. Date of publication September 18, 2017; date of current version December 12, 2017. This work was supported in part by the European Union's Horizon 2020 Research and Innovation Program through the Marie Sklodowska-Curie Grant under Agreement 706334 and in part by the Spanish Ministerio de Economía y Competitividad and European Regional Development Funds under Grant TEC2013-47106-C3. *(Corresponding author: Elena Abdo-Sánchez.)*

E. Abdo-Sánchez is with the Departamento de Ingeniería de Comunicaciones, E.T.S.I. Telecomunicación, Universidad de Málaga, 29010 Málaga, Spain, and also with the Edward S. Rogers Sr. Department of Electrical and Computer Engineering, University of Toronto, Toronto, ON M5S 2E4, Canada (e-mail: elenaabdo@ic.uma.es).

C. Camacho-Peñalosa and T. M. Martín-Guerrero are with the Departamento de Ingeniería de Comunicaciones, E.T.S Ingeniera de Telecomunicación, Universidad de Málaga, 29010 Málaga, Spain (e-mail: ccp@ic.uma.es; teresa@ic.uma.es).

J. Esteban is with the Departamento de Señales, Sistemas y Radiocomunicaciones, E.T.S.I. Telecomunicacíon, Universidad Politécnica de Madrid, 28040 Madrid, Spain (e-mail: jesteban@etc.upm.es).

Color versions of one or more of the figures in this paper are available online at http://ieeexplore.ieee.org.

Digital Object Identifier 10.1109/TMTT.2017.2708103

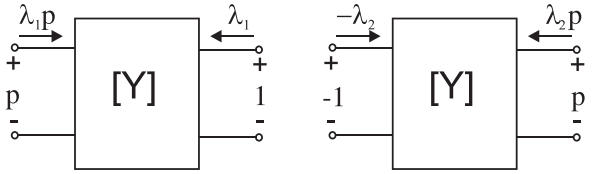

Fig. 1. Interpretation of the eigenvectors of the admittance matrix Y in circuit terms, (a) for $\boldsymbol{v_1} = (1/(p^2+1)^{1/2})[p \;\; 1]^T$ and (b) for $\boldsymbol{v_2} = (1/(p^2+1)^{1/2})[-1 \;\; p]^T$.

series and a single parallel element. Section III deals with the power dissipation in the proposed topologies and proposes a modification in the circuit to achieve power dissipation orthogonality (and, additionally, real transformation ratios for the transformers and nonnegative real parts for the immittances). Section IV shows an example of application of the proposed equivalent circuits to model an asymmetric complementary strip–slot structure. Finally, Section V summarizes the main conclusions.

II. Theory and Derivation

Given the admittance matrix of a general two-port passive reciprocal network with $y_{12} \neq 0$[1]

$$Y = \begin{pmatrix} y_{11} & y_{12} \\ y_{12} & y_{22} \end{pmatrix} \tag{1}$$

its associated eigenvalues are

$$\lambda_1 = \frac{(y_{11}+y_{22}) + \sqrt{(y_{11}-y_{22})^2 + 4y_{12}^2}}{2} \tag{2a}$$

$$\lambda_2 = \frac{(y_{11}+y_{22}) - \sqrt{(y_{11}-y_{22})^2 + 4y_{12}^2}}{2} \tag{2b}$$

and its associated eigenvectors are, respectively, $\boldsymbol{v_1} = (1/(p^2+1)^{1/2})[p \;\; 1]^T$ and $\boldsymbol{v_2} = (1/(p^2+1)^{1/2})[-1 \;\; p]^T$, with

$$p = \frac{(y_{11}-y_{22}) + \sqrt{(y_{11}-y_{22})^2 + 4y_{12}^2}}{2y_{12}}. \tag{3}$$

Then, by the definition of eigenvectors

$$Y\boldsymbol{v_1} = \lambda_1 \boldsymbol{v_1} \tag{4a}$$

$$Y\boldsymbol{v_2} = \lambda_2 \boldsymbol{v_2} \tag{4b}$$

which can be written as

$$\begin{pmatrix} y_{11} & y_{12} \\ y_{12} & y_{22} \end{pmatrix} \begin{pmatrix} p & -1 \\ 1 & p \end{pmatrix} = \begin{pmatrix} \lambda_1 p & -\lambda_2 \\ \lambda_1 & \lambda_2 p \end{pmatrix}. \tag{5}$$

By interpreting (4a) and (4b) in terms of circuits, the eigenvector $\boldsymbol{v_i}$ can be seen as the applied voltages (i.e., p volt applied at port 1 and 1 V at port 2) that generate the currents $\lambda_1 \boldsymbol{v_i}$, as shown in Fig. 1.

Note that (5) can be written as

$$YV = \begin{pmatrix} \lambda_1 \boldsymbol{v_1} & \boldsymbol{0} \end{pmatrix} + \begin{pmatrix} \boldsymbol{0} & \lambda_2 \boldsymbol{v_2} \end{pmatrix} \tag{6}$$

[1]Please note that the derivation for $y_{12} = 0$ is straightforward: $\lambda_1 = y_{11}$ and $\lambda_2 = y_{22}$ and $\boldsymbol{v_1} = [1 \;\; 0]^T$ and $\boldsymbol{v_2} = [0 \;\; 1]^T$ with a trivial equivalent network.

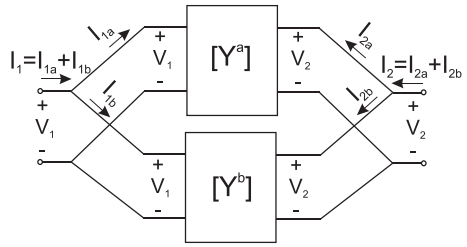

Fig. 2. Decomposition of the network into two subnetworks connected in parallel.

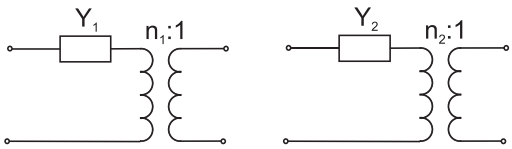

Fig. 3. Proposed *Topology* 1 for (a) subnetwork Y^a and (b) subnetwork Y^b of Fig. 2.

where $V = \{\boldsymbol{v_1} \;\; \boldsymbol{v_2}\}$ is the 2×2 matrix built with the eigenvectors.

Then, the network can be decomposed into two subnetworks connected in parallel (i.e., $Y = Y^a + Y^b$), as shown in Fig. 2, so that

$$Y^a = \begin{pmatrix} \lambda_1 \boldsymbol{v_1} & \boldsymbol{0} \end{pmatrix} V^{-1} \tag{7a}$$

$$Y^b = \begin{pmatrix} \boldsymbol{0} & \lambda_2 \boldsymbol{v_2} \end{pmatrix} V^{-1} \tag{7b}$$

where Y^a and Y^b are the admittance matrices of the corresponding subnetworks. By interpreting again (7a) and (7b) in circuit terms, it can be asserted that the subnetwork Y^a is the resulting network under the excitation $\boldsymbol{v_1} = (1/(p^2+1)^{1/2})[p \;\; 1]^T$, and Y^b the corresponding one under the excitation $\boldsymbol{v_2} = (1/(p^2+1)^{1/2})[-1 \;\; p]^T$.

From (7a) and (7b),

$$[Y^a] = \lambda_1 \begin{pmatrix} \dfrac{p^2}{p^2+1} & \dfrac{p}{p^2+1} \\ \dfrac{p}{p^2+1} & \dfrac{1}{p^2+1} \end{pmatrix} \tag{8a}$$

$$[Y^b] = \lambda_2 \begin{pmatrix} \dfrac{1}{p^2+1} & \dfrac{-p}{p^2+1} \\ \dfrac{-p}{p^2+1} & \dfrac{p^2}{p^2+1} \end{pmatrix}. \tag{8b}$$

A circuit topology that fulfills (8a) must be found. Note that both submatrices have similar expressions and the determinant of both matrices vanishes, which indicates that the corresponding topology cannot have impedance parameters. Additionally, there are only two degrees of freedom, and thus the circuit can have only two complex components. Different topologies have been essayed, and only two alternative circuits have been successfully found. The first one is shown in Fig. 3 and consists of a series admittance cascaded with a transformer for both subnetworks. The second one is similar, but for one of the subnetworks, the locations of the admittance and transformer are exchanged, as shown in Fig. 4.

In order to obtain the parameters of the proposed topologies as a function of the original Y-parameters, the network is

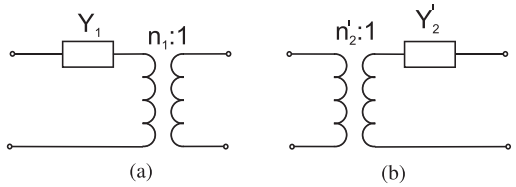

Fig. 4. Proposed *Topology* 2 for (a) subnetwork Y^a and (b) subnetwork Y^b of Fig. 2.

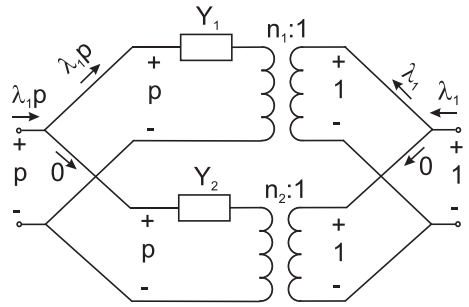

Fig. 5. Excitation of the proposed network with the eigenvector $\boldsymbol{v_1}$.

analyzed when the eigenvectors $\boldsymbol{v_1}$ and $\boldsymbol{v_2}$ are applied as input voltages. It is worth mentioning that, in this paper, the transformation ratios are taken as the ratio between voltages and currents [13, Sec. 8.6], instead of the alternative used by some authors, who define the ratio between voltages as the complex conjugate of the ratio between currents [14, Sec. 2.3].

Fig. 5 shows the first proposed two-port topology under excitation $\boldsymbol{v_1} = (1/(p^2+1)^{1/2})[p \;\; 1]^T$. The current only flows to subnetwork A, on account of the eigenvector orthogonality. Likewise, only the subnetwork B is excited when the voltage applied at the ports of the total network is $\boldsymbol{v_2} = (1/(p^2+1)^{1/2})[-1 \;\; p]^T$. Therefore, the proposed decomposition into subnetworks allows the simplification of the circuit analysis. By solving the circuit network under each eigenstate excitation (as shown in Fig. 5 for $\boldsymbol{v_1}$), the parameters of the proposed networks can be obtained

$$Y_1 = \frac{\lambda_1 p^2}{1+p^2} = p^2 \frac{y_{22} + y_{12} p}{1+p^2} \tag{9a}$$

$$n_1 = \frac{-1}{p} \tag{9b}$$

$$Y_2 = \frac{\lambda_2}{1+p^2} = \frac{p y_{22} - y_{12}}{p(1+p^2)} \tag{9c}$$

$$n_2 = p \tag{9d}$$

$$Y_2' = \frac{\lambda_2 p^2}{1+p^2} = p \frac{p y_{22} - y_{12}}{1+p^2} \tag{9e}$$

$$n_2' = n_2. \tag{9f}$$

The same procedure can be applied to the impedance matrix

$$Z = \begin{pmatrix} z_{11} & z_{12} \\ z_{12} & z_{22} \end{pmatrix} \tag{10}$$

whose eigenvectors are $\boldsymbol{u_1} = (1/(r^2+1)^{1/2})[r \;\; 1]^T$ and $\boldsymbol{u_2} = (1/(r^2+1)^{1/2})[-1 \;\; r]^T$ with

$$r = \frac{(z_{11} - z_{22}) + \sqrt{(z_{11} - z_{22})^2 + 4 z_{12}^2}}{2 z_{12}}. \tag{11}$$

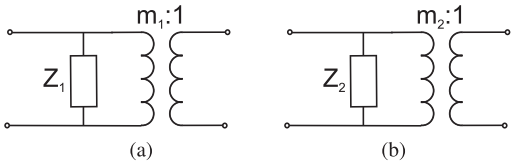

Fig. 6. Proposed *Topology* 3 for (a) subnetwork Z^a and (b) subnetwork Z^b of Fig. 8.

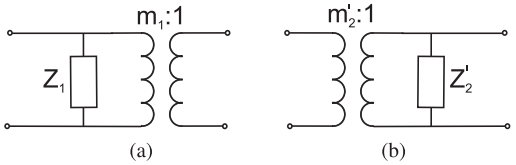

Fig. 7. Proposed *Topology* 4 for (a) subnetwork Z^a and (b) subnetwork Z^b of Fig. 8.

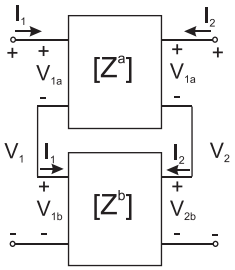

Fig. 8. Decomposition of the network into two subnetworks connected in series.

The following relationship between the eigenvectors of the impedance and admittance matrices can be demonstrated:

$$r = \frac{-1}{p}. \tag{12}$$

Then, two additional topologies for the modeling of a reciprocal network are shown in Figs. 6 and 7, where Z^a and Z^b represent the two subnetworks connected in series, as shown in Fig. 8. Please note that in this case, the eigenvectors are identified with the current excitation and when $\boldsymbol{u_1} = (1/(r^2+1)^{1/2})[r \;\; 1]^T$ is applied as currents, $V_{1b} = V_{2b} = 0$. Analogously, voltages at subnetwork A ports vanish when exciting with $\boldsymbol{u_2}$ currents.

The parameters of these two additional topologies can be obtained in a similar way, thus leading to

$$Z_1 = r^2 \frac{z_{22} + z_{12} r}{1+r^2} \tag{13a}$$

$$m_1 = r \tag{13b}$$

$$Z_2 = \frac{r z_{22} - z_{12}}{r(1+r^2)} \tag{13c}$$

$$m_2 = \frac{-1}{r} \tag{13d}$$

$$Z_2' = r \frac{r z_{22} - z_{12}}{1+r^2} \tag{13e}$$

$$m_2' = m_2. \tag{13f}$$

Therefore, the expressions for the parameters obtained for the topologies shown in Figs. 6 and 7 are similar to the ones for the topologies shown in Figs. 3 and 4, with the difference that the former is expressed as a function of the Z-parameters and the latter of the Y-parameters.

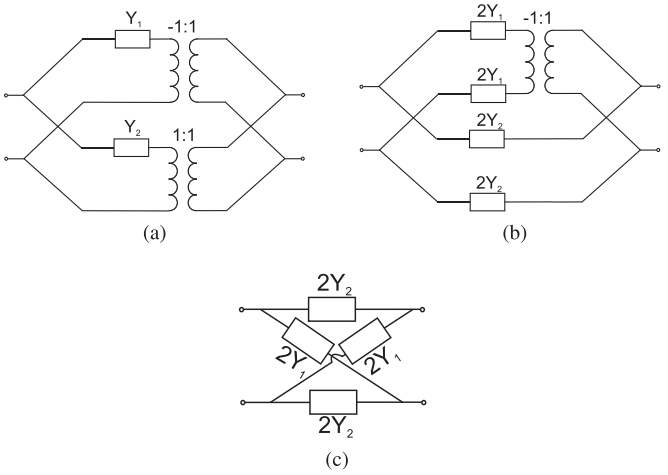

Fig. 9. Different representations of the proposed *Topology* 1 for the symmetric case. Degeneration in a lattice network. (a) Step 1. (b) Step 2. (c) Step 3 (lattice network).

A. Symmetric Case: The Lattice Network

For a symmetric network ($y_{11} = y_{22}$), $p = 1$, and thus the eigenvectors $\boldsymbol{v_1} = (1/\sqrt{2})[1\ \ 1]^T$ and $\boldsymbol{v_2} = (1/\sqrt{2})[-1\ \ 1]^T$ correspond to the odd and even excitations, respectively. Then, according to Bartlett's theorem [7], it can be expected that the proposed circuit degenerates in a lattice network as shown in Fig. 9 for *Topology* 1 (the same applies for *Topology* 2). In fact, by applying symmetry to (9)

$$Y_1 = \frac{y_{11} + y_{12}}{2} \tag{14a}$$

$$Y_2 = Y_2' = \frac{y_{11} - y_{12}}{2} \tag{14b}$$

$$n_1 = -1 \tag{14c}$$

$$n_2 = n_2' = 1 \tag{14d}$$

so that the obtained series-branch admittance $2Y_2$ and the cross-branch admittance $2Y_1$ of the lattice network of Fig. 9(c) agree with the general lattice expressions [1].

For *Topologies* 3 and 4 (with the impedance matrix), the following parameters are obtained:

$$Z_1 = \frac{z_{11} + z_{12}}{2} \tag{15a}$$

$$Z_2 = Z_2' = \frac{z_{11} - z_{12}}{2} \tag{15b}$$

$$m_1 = 1 \tag{15c}$$

$$m_2 = m_2' = -1. \tag{15d}$$

By converting the impedance parameters in (15) to admittance parameters, the following relations between *Topologies* 1 (or 2) and 3 (or 4) can be demonstrated:

$$Z_1 = \frac{1}{4Y_1} \tag{16a}$$

$$Z_2 = Z_2' = \frac{1}{4Y_2}. \tag{16b}$$

Therefore, *Topologies* 3 and 4 also degenerate for the symmetric case in a lattice network with series-branch impedance $2Z_2$ and cross-branch impedance $2Z_1$.

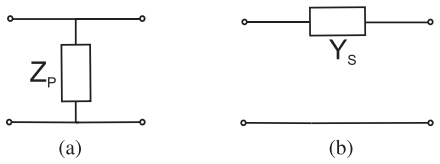

Fig. 10. Topologies for the analyzed special cases. (a) Parallel element. (b) Series element.

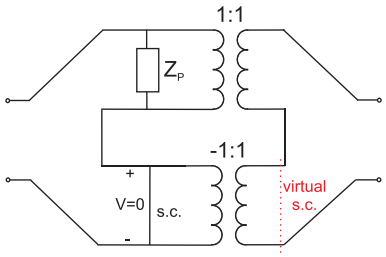

Fig. 11. *Topology 3* for the special case of a parallel element. "s.c." stands for short circuit.

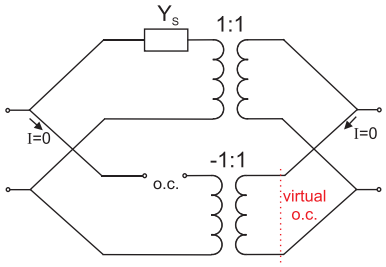

Fig. 12. *Topology 1* for the special case of a series element. "o.c." stands for open circuit.

B. Special Cases: Series and Parallel Elements

In order to show the consistency of the proposed topologies and expressions, two special cases are analyzed in this section: the parallel, Z_P, and series element, Y_S (Fig. 10). The fact that the proposed topologies degenerate in its corresponding equivalent circuits is shown in the following.

1) Parallel Element: In this case, it is straightforward to demonstrate that the eigenvalues of the impedance matrix and its corresponding eigenvectors are given by

$$\lambda_1 = 2Z_P \qquad \lambda_2 = 0 \tag{17a}$$

$$r = 1. \tag{17b}$$

Then, for this particular case, *Topology* 3 results in the circuit shown in Fig. 11, which certainly corresponds to the circuit of Fig. 10(a).

2) Series Element: Likewise, for a series element, the resulting eigenvalues of the admittance matrix and its corresponding eigenvectors are given by

$$\lambda_1 = 2Y_S \qquad \lambda_2 = 0 \tag{18a}$$

$$p = -1. \tag{18b}$$

Then, for this particular case, *Topology* 1 results in the circuit shown in Fig. 12, which likewise corresponds to the circuit of Fig. 10(b).

III. Power Dissipation

The power dissipated in any two-port network is given by

$$P_{\text{dis}} = \frac{1}{2}\text{Re}\{V_1 I_1^* + V_2 I_2^*\}. \tag{19}$$

Then, by applying the excitation given by the eigenvector $(1/(p^2+1)^{1/2})[p \;\; 1]^T$ to the two-port network of admittance matrix $[Y]$, the dissipated power is

$$P_{\text{dis}}{}^a = \frac{1}{2}\text{Re}\left\{\frac{|p|^2+1}{p^2+1}\lambda_1\right\}. \tag{20}$$

Likewise, by applying the excitation given by the eigenvector $(1/(p^2+1)^{1/2})[-1 \;\; p]^T$, the dissipated power is

$$P_{\text{dis}}{}^b = \frac{1}{2}\text{Re}\left\{\frac{|p|^2+1}{p^2+1}\lambda_2\right\}. \tag{21}$$

An arbitrary excitation $[V_1 \;\; V_2]^T$ can then be written as a linear combination of the two previous eigenvectors

$$\begin{pmatrix} V_1 \\ V_2 \end{pmatrix} = A\begin{pmatrix} p \\ 1 \end{pmatrix} + B\begin{pmatrix} -1 \\ p \end{pmatrix} \tag{22}$$

from which A and B are obtained as

$$A = \frac{pV_1 + V_2}{\sqrt{p^2+1}} \tag{23a}$$

$$B = \frac{pV_2 - V_1}{\sqrt{p^2+1}}. \tag{23b}$$

The currents through ports 1 and 2 can then be written as

$$\begin{pmatrix} I_1 \\ I_2 \end{pmatrix} = A\begin{pmatrix} p\lambda_1 \\ \lambda_1 \end{pmatrix} + B\begin{pmatrix} -\lambda_2 \\ p\lambda_2 \end{pmatrix}. \tag{24}$$

Therefore, it is straightforward to obtain the power dissipated in the two-port network, which results in

$$P_{\text{dis}} = \frac{1}{2}\left[|A|^2\text{Re}\left\{\frac{|p|^2+1}{p^2+1}\lambda_1\right\} + |B|^2\text{Re}\left\{\frac{|p|^2+1}{p^2+1}\lambda_2\right\}\right] + \frac{1}{2}\text{Re}\left\{AB^*\frac{-p+p^*}{p^2+1}\lambda_1 + A^*B\frac{p-p^*}{p^2+1}\lambda_2\right\} \tag{25}$$

which corresponds to

$$P_{\text{dis}} = |A|^2 P_{\text{dis}}{}^a + |B|^2 P_{\text{dis}}{}^b + \text{Im}\{p\}\text{Re}\left\{j\frac{-AB^*\lambda_1 + A^*B\lambda_2}{p^2+1}\right\}. \tag{26}$$

This result indicates that, in the general case, there is some interaction between the two modes. It means that the power dissipated in submatrix $[Y^a]$ when it is connected in parallel to submatrix $[Y^b]$ (modeling a general admittance matrix $[Y]$) is different than when it is isolated ($[Y] = [Y^a]$), and the same applies to $[Y^b]$. However, when p is a real number, power orthogonality of the modes associated with the eigenvectors is achieved and, in addition, according to (9), the transformation ratios of the transformers become real.

According to (3), the power orthogonality happens in each of the following cases:

1) if $[Y]$ is purely imaginary (lossless case);
2) if $[Y]$ is purely real;
3) if $[Y]$ corresponds to a symmetric network.

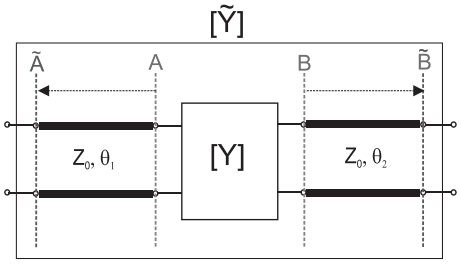

Fig. 13. Required shift in the reference planes to guarantee power dissipation orthogonality. The proposed equivalent-circuit extraction procedure is applied to the resulting $[\tilde{Y}]$.

The last case leads to the same conclusion as that stated in [9] about the power dissipation independence in the branches of a lattice network. In fact, the power orthogonality applied to the symmetric case means that the power dissipated in the part of the circuit corresponding to submatrix $[Y^a]$ (one of the lattice branches) is independent on the value of $[Y^b]$ (the other branch) and vice versa.

A. Enforcing Power Orthogonality

In order to force the transformation ratio to be real, and hence, ensuring power dissipation independence, a phase shift of the two-port parameters can be applied by changing the reference planes accordingly. In the following, the details of this process are presented for *Topology* 1, although the same procedure can be applied to the other proposed topologies.

In order to obtain transformers with real transformation ratios, p must be real according to (9). If p is expressed in terms of the S-parameters (with a reference impedance Z_0), the following expression is obtained:

$$p = \frac{(s_{11}-s_{22}) - \sqrt{(s_{11}-s_{22})^2 + 4s_{12}^2}}{2s_{12}} \tag{27}$$

which can also be written as

$$p = \frac{s_{11}-s_{22}}{2s_{12}} - \sqrt{\left(\frac{s_{11}-s_{22}}{2s_{12}}\right)^2 + 1}. \tag{28}$$

Then, a sufficient condition for p to be real is that $(s_{11} - s_{22}/2s_{12})$ is also real.

If the reference planes are moved along two ideal transmission lines of electrical lengths θ_1 and θ_2 at ports 1 and 2, respectively, as shown in Fig. 13, the condition for a real transformation ratio results

$$\text{Im}\left[\frac{s_{11}e^{-j2\theta_1} - s_{22}e^{-j2\theta_2}}{2s_{12}e^{-j(\theta_1+\theta_2)}}\right] = 0 \tag{29}$$

which has the following solution:

$$\Delta\theta = \arg(s_{12}^* s_{11} + s_{12}s_{22}^*) \tag{30}$$

where $\Delta\theta = \theta_1 - \theta_2$ is the difference in electrical length between the shifts of the reference planes. Please note that (30) is indeterminate for the lossless case (i.e., $\Delta\theta$ can take any value). Therefore, the determination of $\Delta\theta$ might be problematic in the low-loss case. In fact, measurement errors could lead to high variations in its value.

Therefore, by choosing properly the reference planes of the structure to model (transforming $[Y]$ into $[\tilde{Y}]$, see Fig. 13), transformers with real transformation ratios can be obtained. Moreover, there is an extra degree of freedom, since only the difference between the electrical lengths is imposed, but not their independent values. Please note that the shift in the reference planes is equivalent to adding any two ideal transmission line sections that satisfy (30)—with opposite sign for $\Delta\theta$—at the input and output ports of the chosen topology. In this way, if the reference planes are fixed, the final equivalent circuit of $[Y]$ would consist of the chosen topology (*Topologies* 1–4 in Section II) along with the corresponding transmission line sections.

B. Immittances With Nonnegative Real Parts

According to the energy theorem, the admittance and impedance matrices must fulfill the following conditions [1], [6]:

$$r_{11}r_{22} - r_{12}^2 \geq 0 \tag{31a}$$

$$r_{11} \geq 0 \tag{31b}$$

$$r_{22} \geq 0 \tag{31c}$$

where r_{ij} is the real part of y_{ij}, or equivalently the real part of z_{ij}.

The admittance parameters of the network in Fig. 2 with *Topology* 1 can be easily obtained by circuit analysis as

$$\tilde{y}_{11} = Y_1 + Y_2 \tag{32a}$$

$$\tilde{y}_{12} = -n_1 Y_1 + \frac{1}{n_1} Y_2 \tag{32b}$$

$$\tilde{y}_{22} = n_1^2 Y_1 + \frac{1}{n_1^2} Y_2 \tag{32c}$$

in which the relationship $n_2 = -(1/n_1)$ has been used.

By introducing (32) into condition (31a) and considering n_1 real, (31a) is reduced to

$$\mathrm{Re}[Y_1]\mathrm{Re}[Y_2]\left(n_1 + \frac{1}{n_1}\right)^2 \geq 0. \tag{33}$$

Then, the following condition must be satisfied:

$$\mathrm{Re}[Y_1]\mathrm{Re}[Y_2] \geq 0 \tag{34}$$

which can be achieved with both $\mathrm{Re}[Y_1]$ and $\mathrm{Re}[Y_2]$ simultaneously positive or negative. However, introducing (32) into conditions (31b) and (31c) leads to

$$\mathrm{Re}(Y_1 + Y_2) \geq 0 \tag{35a}$$

$$\mathrm{Re}\left(n_1^2 Y_1 + \frac{1}{n_1^2} Y_2\right) \geq 0 \tag{35b}$$

which forces the only solution to be $\mathrm{Re}[Y_1] \geq 0$ and $\mathrm{Re}[Y_2] \geq 0$ simultaneously, thus guaranteeing admittances with nonnegative real parts for the proposed topology.

In *Topology 2*, condition (31a) leads to

$$4\mathrm{Re}[Y_1]\mathrm{Re}[Y_2'] \geq 0 \tag{36}$$

which, together with (31b) and (31c), also forces $\mathrm{Re}[Y_1] \geq 0$ and $\mathrm{Re}[Y_2'] \geq 0$.

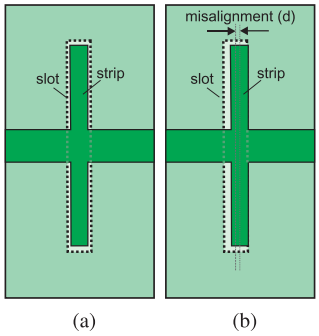

Fig. 14. (a) Symmetric (aligned) strip–slot structure. (b) Asymmetric (misaligned) strip–slot structure.

By analogy, the same can be proven for *Topology* 3 and *Topology* 4. In fact, the Z-parameters of *Topology* 3 are the following:

$$\tilde{z}_{11} = Z_1 + Z_2 \tag{37a}$$

$$\tilde{z}_{12} = \frac{1}{m_1} Z_1 - m_1 Z_2 \tag{37b}$$

$$\tilde{z}_{22} = \frac{1}{m_1^2} Z_1 + m_1^2 Z_2 \tag{37c}$$

in which the relationship $m_2 = -(1/m_1)$ has been used. The previous expressions are analogous to (32), and so are the Z-Parameters of *Topology* 4 with respect to the Y-Parameters of *Topology* 2.

IV. Results

In order to illustrate the usefulness of the proposed topologies with a real structure, the aforementioned equivalent circuits have been extracted for a planar structure called *the complementary strip–slot element*. This structure has been chosen, because its intrinsic equivalent circuit is a lattice network, as demonstrated in [15]. It consists of a slot etched on the ground plane of a microstrip line and its complementary stub (or strip) aligned to it on the microstrip layer and transversely fed by the microstrip (of characteristic impedance $Z_0 = 1/Y_0 = 50\ \Omega$), as shown in Fig. 14(a). In [16], the strip–slot structure was asymmetrized [through a horizontal misalignment between the slot and the strip, as shown in Fig. 14(b)] to be proposed as an alternative unit cell for leaky-wave antennas scanning through broadside. However, although the equivalent circuit for the symmetric structure was demonstrated to be a symmetric lattice network, no such equivalence was found for its asymmetrized counterpart at that moment. Moreover, due to the association of the branches of the symmetric lattice with the even and odd excitation modes, the strip–slot modeled with this topology provides an important physical insight, since the slot can be associated with the odd mode and the strip to the even mode. Therefore, the impedances of the lattice branches represent separately the strip and the slot [9], [15].

A series of prototypes with dimensions as in [16], but with different misalignments, were fabricated and measured in the N5247A PNA-X Network Analyzer from Agilent Technologies, using TRL calibration. Fig. 15(a) and (b)

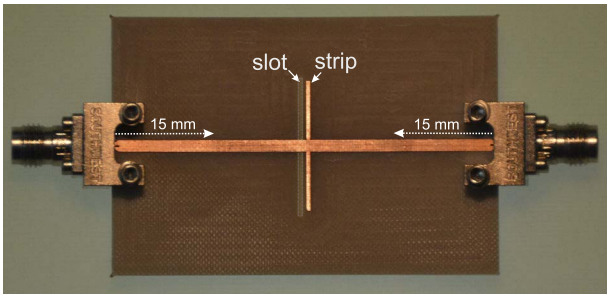

(a)

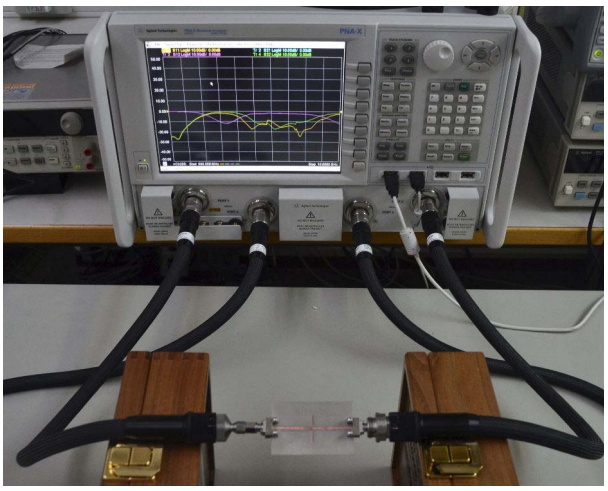

(b)

Fig. 15. (a) Partially backlit photograph of one of the prototypes taken from the side of the strip layer, so that the slot etched on the ground plane is noticeable. It corresponds to a degree of misalignment of $d = 1080$ μm. The reference planes are located 15 mm away from the launchers, as indicated. (b) Photograph of the measurement setup.

shows the photographs of the prototype with the strongest misalignment ($d = 1080$ μm) indicating the location of the reference planes and the measurement setup, respectively. The TRL calibration was done with three "Lines" to cover the whole band of interest. Some anomalies are expected at the frequencies where the calibration switches from one "Line" to another. The worst situation happens around 9.4 GHz. Therefore, the most evident anomalies will be seen in the following results around this frequency point.

Results obtained from the measurements for *Topology* 1 of the strip slot with different degrees of asymmetry are provided in the following. The values for the parameters of the other topologies are omitted here, for simplicity. As a first step, the results of (9a)–(9c) without shift in the reference planes are shown in Figs. 16–19 (real and imaginary parts). It is worth mentioning that a degree of misalignment of $d = 540$ μm for the analyzed geometry makes the strip and the slot have no overlapping area (they are adjacent elements loading the microstrip), whereas $d = 0$ corresponds to the symmetric case. The admittances respond to the natural behavior of the short- and open-circuited stubs, which are the equivalent circuits associated with the slot and the strip, respectively [15].

The transformation ratio of the corresponding transformer, n_1, is plotted in Figs. 18 (real part) and 19 (imaginary part). The simulation results (obtained

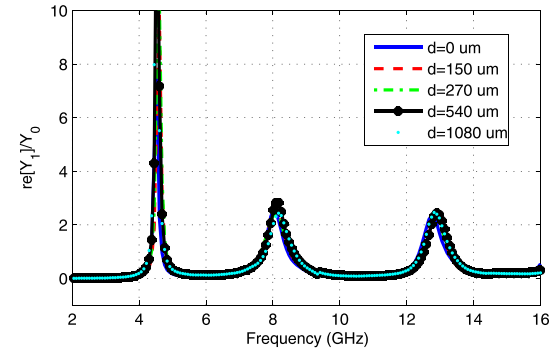

(a)

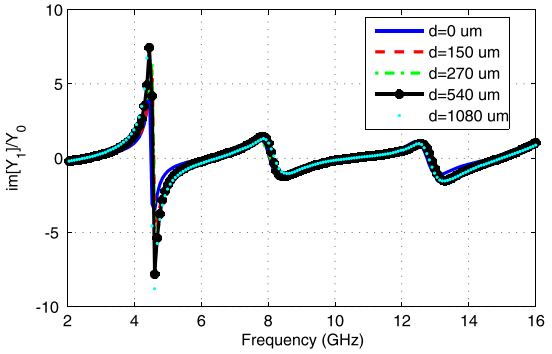

(b)

Fig. 16. (a) Real and (b) imaginary parts of the normalized Y_1 for the measured complementary strip–slot with different misalignments.

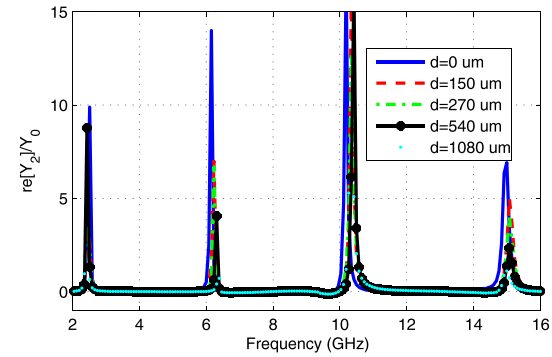

(a)

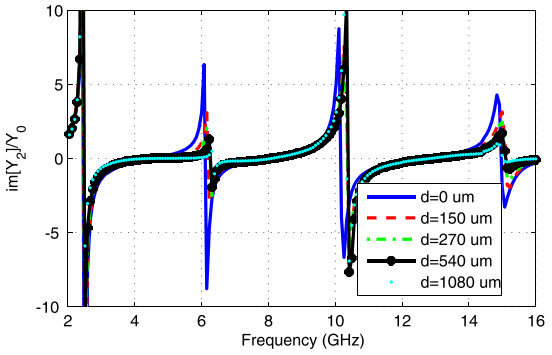

(b)

Fig. 17. (a) Real and (b) imaginary parts of the normalized Y_2 for the measured complementary strip–slot with different misalignments.

with HFSS) are also plotted here, in order to show how the results would look like without the ripples due to measurement errors. The same behavior is achieved for

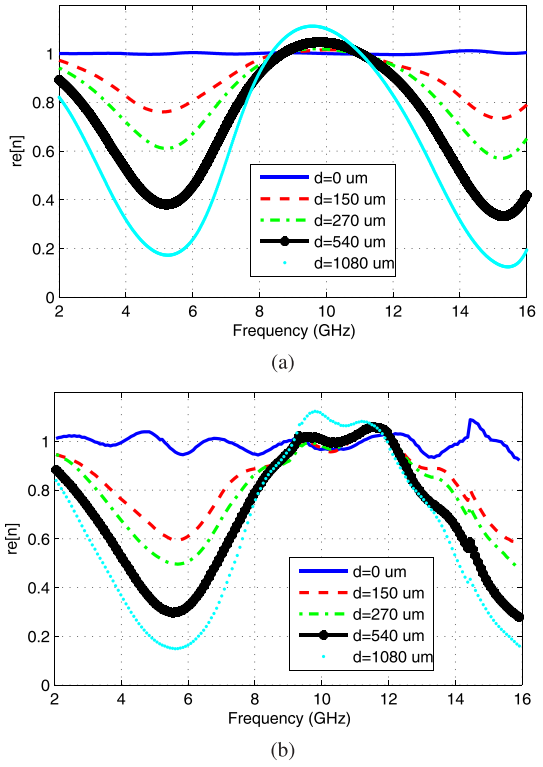

Fig. 18. Real part of n for the complementary strip–slot with different misalignments. (a) Simulations. (b) Measurements.

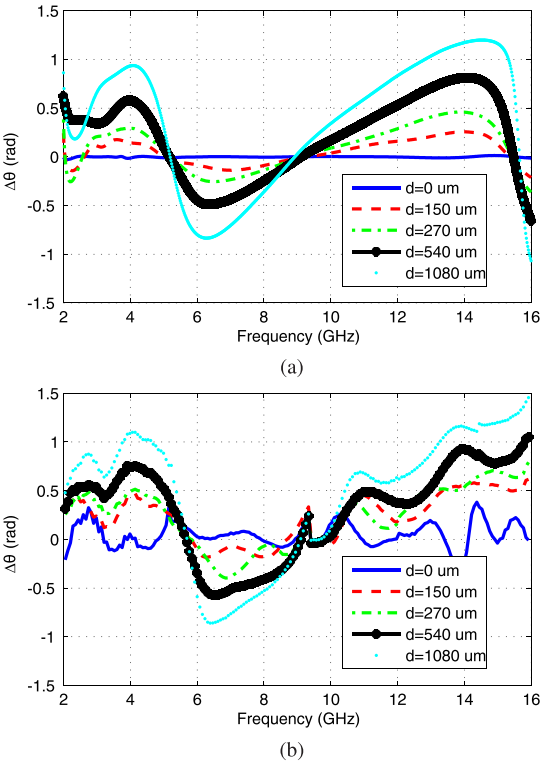

Fig. 20. Required differential shift in the reference planes $\Delta\theta = \theta_1 - \theta_2$ for realizability of the transformers for the complementary strip–slot with different misalignments. (a) Simulations. (b) Measurements.

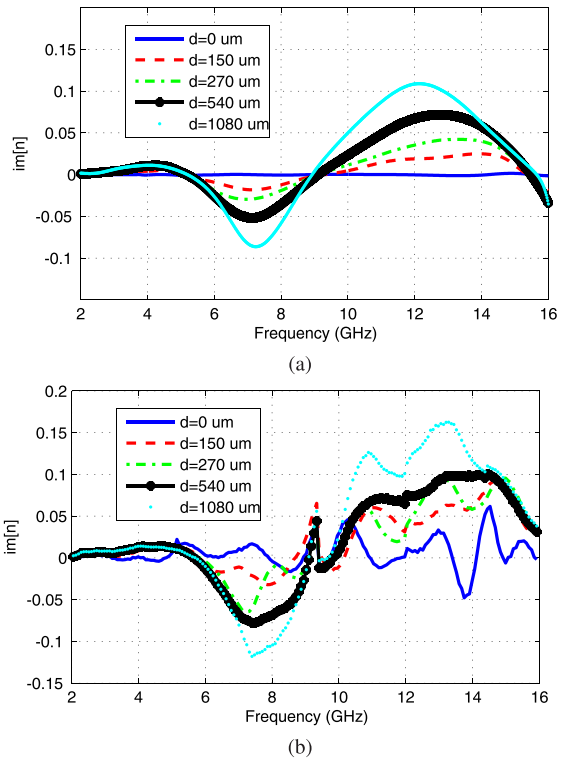

Fig. 19. Imaginary part of n for the complementary strip–slot with different misalignments. (a) Simulations. (b) Measurements.

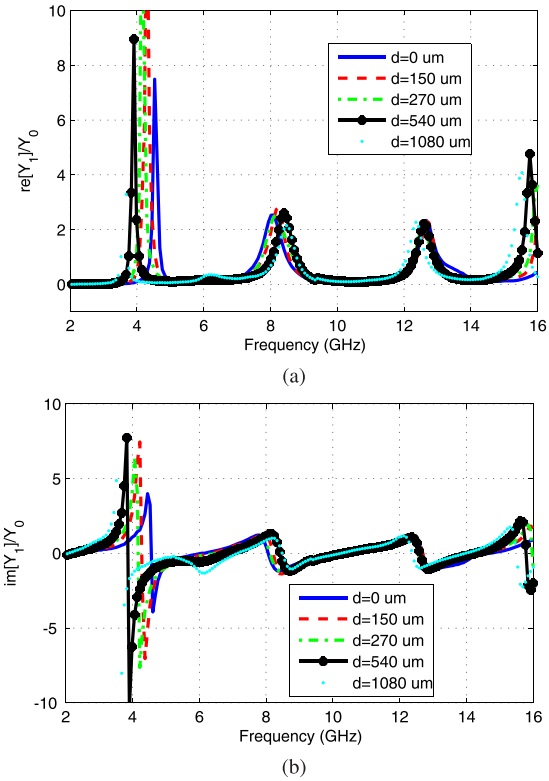

Fig. 21. (a) Real and (b) imaginary parts of the normalized Y_1 with a shift in the reference planes for the measured complementary strip–slot with different misalignments.

both the simulations and measurements. Moreover, it can be observed that the asymmetry mainly affects the real part of the transformation ratio among all the parameters. Although the imaginary parts of the transformation ratios for the analyzed misalignments are rather small, they are complex numbers.

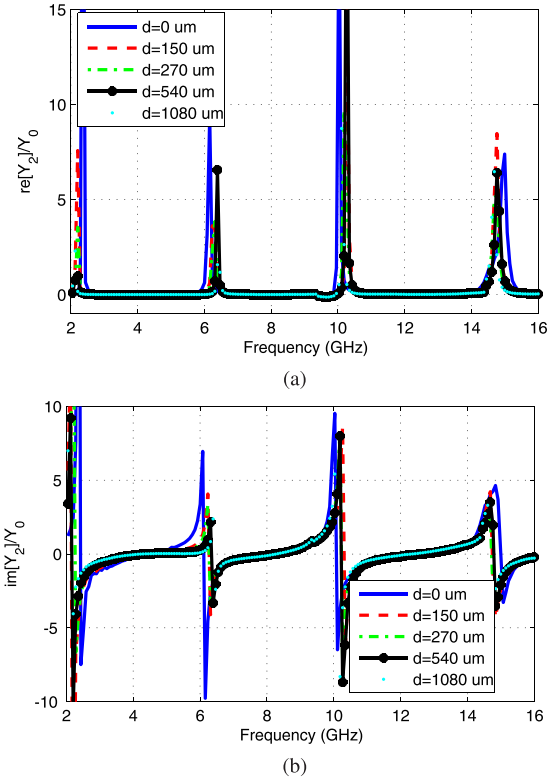

Fig. 22. (a) Real and (b) imaginary parts of the normalized Y_2 with a shift in the reference planes for the measured complementary strip–slot with different misalignments.

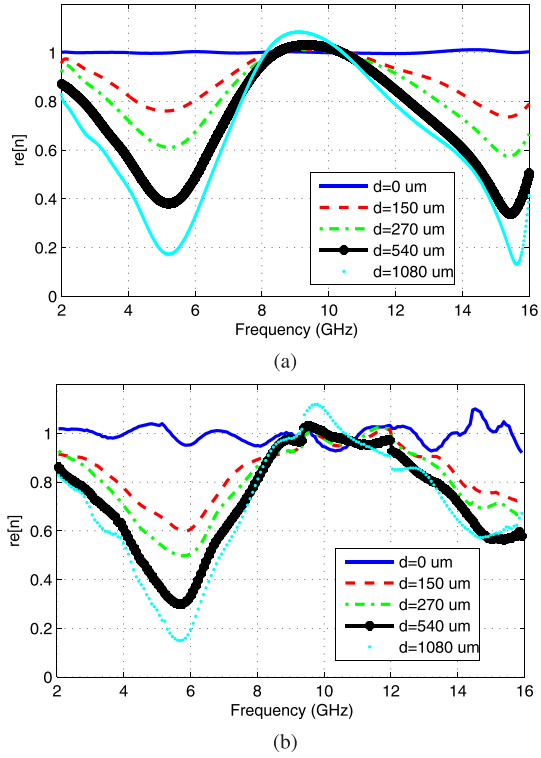

Fig. 23. Real part of n with a shift in the reference planes for the complementary strip–slot with different misalignments. (a) Simulations. (b) Measurements.

The admittance values of the branches of the equivalent circuit are slightly sensitive to the asymmetry of the structure. This is of relevant importance, since it means that, even with significant misalignments of 100% ($d = 540$ μm) or 200% ($d = 1080$ μm), the impedances of the proposed equivalent circuit still represent properly the slot and the strip, separately, as the cross and parallel branches in the symmetric case. In fact, this is consistent with the property related to the eigenstates for the derived topologies, since the slot can still be associated with the quasi-odd-mode and the strip to the quasi-even-mode excitations.

As demonstrated in Section III, power dissipation orthogonality (and transformers with real transformation ratios as well as nonnegative real parts for the admittances) can be guaranteed by introducing a shift in the reference planes. Following (30), the required phase shift difference between the two ports, $\Delta\theta = \theta_1 - \theta_2$, has been calculated for each frequency and is plotted in Fig. 20. Although this parameter is frequency-dependent, it has a smooth variation with frequency. Anyway, it is important to point out that moving the reference planes over frequency is customary in the extraction of equivalent circuits, as, for instance, in [17] and [18]. As expected, the more asymmetry is introduced in the structure, the higher is the "asymmetry" in the reference planes required to compensate the imaginary part of the transformation ratio. Both simulations and measurements show again the same behavior.

In order to check whether the theory is correct and the introduction of a specific difference in the shift of the reference planes makes the transformation ratios real and the real parts of the admittances nonnegative, Figs. 21–23 show the new parameters for *Topology* 1 after applying the shift in the reference planes given by Fig. 20. Since only the difference $\theta_1 - \theta_2$ must be set, there is still a degree of freedom. Thus, the shift has been applied only to one of the ports leaving the other port without shift. The resulting admittances have a similar behavior to those obtained without reference shift. Nonnegative real parts for the admittances are obtained, as predicted by the theory, over the whole bandwidth except for a small region between 9 and 10 GHz, where the real part of Y_2 takes slightly negative values. However, Fig. 20(b) shows that there is an anomalous behavior in the measurements over this frequency region that does not appear in simulations [Fig. 20(a)]. Therefore, it can be concluded that this response is due to artifacts from the measurements, related with the previously mentioned TRL calibration errors.

The main difference between the results with and without shift in the reference planes is obtained in the transformation ratio, since now real values are achieved for the whole bandwidth. Imaginary parts for n in the order of 10^{-8} and 10^{-3} or below are obtained for the simulations and measurements, respectively. Moreover, since the admittances do not change significantly, it seems that it is essentially in the transformer where the asymmetry is absorbed.

V. Conclusion

Novel circuit topologies have been proposed as an extension of the symmetric lattice network for asymmetric structures. The derivation of the proposed networks has been made by using an eigenstate formulation approach. In this way,

two connected (in series or in parallel) subnetworks are obtained, each one associated with a different eigenstate. The derived admittance matrix for these subnetworks constrains the network topologies that can be used. Four topologies have been proposed. These topologies degenerate in the symmetric lattice network for symmetric immittance matrices and in parallel and series elements for their corresponding matrices.

Since the eigenstate separation is implicit in the formulation, the derived asymmetric topologies preserve this property of symmetric lattice networks. The power dissipation analysis has allowed the derivation of the independence power dissipation property of symmetric lattice networks as a particular case. Moreover, it has been shown that, by properly choosing the reference planes, the feature of power orthogonality of symmetric lattice networks is also achieved for the asymmetric topologies. With this modification in the reference planes, the transformation ratios for the transformers become real and the real parts of the admittances nonnegative, as desired for a proper modeling. Additionally, only the shift difference between the reference planes at the input and the output is imposed, which provides an additional degree of freedom to set one of the reference planes wherever it is desired.

An illustrative example has been provided, extracting the equivalent circuit of a complementary strip–slot with different degrees of asymmetry. The symmetric structure has a symmetric lattice network as equivalent circuit, with the branches representing the slot and the strip separately (odd and even modes, respectively). This same separation is to some extent maintained by the proposed topologies when the structure is asymmetrized, being mainly the transformation ratios of the transformers the parameters that change with the degree of asymmetry. Although some differences are found in the admittances of the asymmetric structures with respect to the symmetric case, their behaviors are well preserved. The proposed equivalent circuit shows a very good behavior with smooth frequency variation of its parameters over a broad bandwidth.

The derived theory is powerful, since it could be extended to n-ports, except for the complexity in the mathematical derivation. The difficulty will lie in finding the topologies to implement the resulting subnetworks. Future work will be carried out to apply the proposed topologies to other asymmetric structures and check whether the transformation ratios are the parameters where most of the effects of the asymmetry can be accounted for.

ACKNOWLEDGMENT

The authors would like to thank Prof. F. Mesa, Universidad de Sevilla, Seville, Spain, for the fruitful discussions about the lattice network and the provided reference [12], which has been the source of inspiration for this paper.

REFERENCES

[1] M. E. Van Valkenburg, *Introduction to Modern Network Synthesis*. New York, NY, USA: Wiley, 1960.

[2] J. Esteban, C. Camacho-Peñalosa, J. E. Page, and T. M. Martín-Guerrero, "Generalized lattice network-based balanced composite right-/left-handed transmission lines," *IEEE Trans. Microw. Theory Techn.*, vol. 60, no. 8, pp. 2385–2393, Aug. 2012.

[3] F. Bongard and J. R. Mosig, "A novel composite right/left-handed unit cell and potential antenna applications," in *Proc. IEEE Antennas Propag. Soc. Int. Symp.*, Jul. 2008, pp. 1–4.

[4] F. Bongard, J. Perruisseau-Carrier, and J. Mosig, "Enhanced CRLH transmission line performances using a lattice network unit cell," *IEEE Microw. Wireless Compon. Lett.*, vol. 19, no. 7, pp. 431–433, Jul. 2009.

[5] J. E. Page, J. Esteban, and C. Camacho-Peñalosa, "Lattice equivalent circuits of transmission-line and coupled-line sections," *IEEE Trans. Microw. Theory Techn.*, vol. 59, no. 10, pp. 2422–2430, Oct. 2011.

[6] C. G. Montgomery, R. H. Dicke, and E. M. Purcell, Eds., *Principles of Microwave Circuits*. New York, NY, USA: McGraw-Hill, 1950.

[7] A. C. Bartlett, *The Theory of Electrical Artificial Lines and Filters*. New York, NY, USA: Wiley, 1930, pp. 28–32.

[8] E. Abdo-Sánchez, J. Esteban, T. M. Martín-Guerrero, J. E. Page, and C. Camacho-Peñalosa, "The use of lattice networks for modelling symmetric transmission line components and discontinuities," *Microw. Opt. Technol. Lett.*, vol. 55, pp. 636–639, Mar. 2013.

[9] E. Abdo-Sánchez, T. M. Martín-Guerrero, J. Esteban, and C. Camacho-Peñalosa, "On the radiation properties of the complementary strip-slot element," *IEEE Antennas Wireless Propag. Lett.*, vol. 14, pp. 1389–1391, 2015.

[10] S. Otto, A. Rennings, K. Solbach, and C. Caloz, "Transmission line modeling and asymptotic formulas for periodic leaky-wave antennas scanning through broadside," *IEEE Trans. Antennas Propag.*, vol. 59, no. 10, pp. 3695–3709, Oct. 2011.

[11] S. Otto, A. Al-Bassam, A. Rennings, K. Solbach, and C. Caloz, "Transversal asymmetry in periodic leaky-wave antennas for bloch impedance and radiation efficiency equalization through broadside," *IEEE Trans. Antennas Propag.*, vol. 62, no. 10, pp. 5037–5054, Oct. 2014.

[12] S. Wane and D. Bajon, "Broadband equivalent circuit derivation for multi-port circuits based on eigen-state formulation," in *IEEE MTT-S Int. Microw. Symp. Dig.*, Boston, MA, USA, Jun. 2009, pp. 305–308.

[13] G. Zeveke, P. Ionkin, A. Neutushil, and S. Strakhov, "Multi and two-ports with sinusoidal current and voltage," in *Analysis and Synthesis of Electric Circuits*. Moskow, Russia: MIR, 1979.

[14] P. Kundur, "Phase-shifting transformers," in *Power System Stability and Control*. New York, NY, USA: McGraw-Hill, 1993.

[15] E. Abdo-Sánchez, J. E. Page, T. M. Martín-Guerrero, J. Esteban, and C. Camacho-Peñalosa, "Planar broadband slot radiating element based on microstrip-slot coupling for series-fed arrays," *IEEE Trans. Antennas Propag.*, vol. 60, no. 12, pp. 6037–6042, Dec. 2012.

[16] E. Abdo-Sánchez, T. M. Martín-Guerrero, J. Esteban, and C. Camacho-Peñalosa, "Short dual-band planar leaky-wave antenna with broadside effect mitigation," *IET Microw., Antennas Propag.*, vol. 10, no. 5, pp. 574–578, Apr. 2016.

[17] L. B. Felsen and A. A. Oliner, "Determination of equivalent circuit parameters for dissipative microwave structures," *Proc. IRE*, vol. 42, no. 2, pp. 477–483, Feb. 1954.

[18] E. Hammerstad, "Computer-aided design of microstrip couplers with accurate discontinuity models," in *IEEE MTT-S Int. Microw. Symp. Dig.*, Jun. 1981, pp. 54–56.

Elena Abdo-Sánchez (M'17) received the M.Sc. and Ph.D. degrees in telecommunication engineering from the Universidad de Málaga, Málaga, Spain, in 2010 and 2015, respectively.

In 2009, she was a Granted Student with the German Aerospace Center, Institute of Communications and Navigation, Munich, Germany. In 2010, she joined the Department of Communication Engineering, Universidad de Málaga, as a Research Assistant. In 2013, she was a Visiting Ph.D. Student with the Antennas and Applied Electromagnetics Laboratory, University of Birmingham, Birmingham, U.K. From 2016 to 2017, she was a Marie Sklodowska-Curie Post-Doctoral Fellow with the Electromagnetics Group, University of Toronto, Toronto, ON, Canada. She is currently a Post-Doctoral Fellow with the University of Málaga. Her current research interests include the electromagnetic analysis and design of planar antennas and the application of metasurfaces to the implementation of novel antennas.

Dr. Abdo-Sánchez was a recipient of the Junta de Andalucía Scholarship from 2012 to 2015 and the Marie Sklodowska-Curie Fellowship from 2016 to 2018.

Carlos Camacho-Peñalosa (S'80–M'82–SM'16) received the Ingeniero de Telecomunicación and Dr.-Ing. degrees from the Universidad Politécnica de Madrid, Madrid, Spain, in 1976 and 1982, respectively.

From 1976 to 1989, he was with the Escuela Técnica Superior de Ingenieros de Telecomunicación, Universidad Politécnica de Madrid, as a Research Assistant, an Assistant Professor, and an Associate Professor. From 1984 to 1985, he was a Visiting Researcher with the Department of Electronics, Chelsea College, University of London, London, U.K. In 1989, he became a Full Professor with the University of Málaga, Málaga, Spain. He was the Director of the Escuela Técnica Superior de Ingeniería de Telecomunicación from 1991 to 1993. He was with the University of Málaga, as the Vice-Rector from 1993 to 1994, the Deputy Rector in 1994, and the Director with the Departamento de Ingeniería de Comunicaciones, from 1996 to 2004. From 2000 to 2003, he was the Co-Head of the Nokia Mobile Communications Competence Centre, Málaga. He has been responsible for several research projects on nonlinear microwave circuit analysis, microwave semiconductor device modeling, and applied electromagnetics. His current research interests include microwave and millimeter solid-state circuits, nonlinear systems, and applied electromagnetism.

Teresa M. Martín-Guerrero was born in Málaga, Spain. She received the Grado de Licenciado en Ciencias Físicas (M.Sc. equivalent in physics) from the Universidad de Granada, Granada, Spain, in 1990, and the Grado de Doctor Ingeniero de Telecomunicación (Ph.D. equivalent in telecommunication engineering) from the Universidad de Málaga, Málaga, in 1995.

In 1991, she joined the Departamento de Ingenieria de Comunicaciones, Universidad de Málaga, where she became a Full Professor in 2016. From 2008 to 2012, she was the Vice-Director for Research with the E.T.S Ingeniera de Telecomunicación (Faculty of Telecommunication Engineering), Universidad de Málaga. Her current research interests include microwave and millimeter-wave device modeling, analysis, and design of RF power amplifiers.

Jaime Esteban received the Ingeniero de Telecomunicacíon and Dr.Eng. degrees from the Universidad Politécnica de Madrid, Madrid, Spain, in 1987 and 1990, respectively.

From 1988 to 2014, he was with the Departamento de Electromagnetismo y Teoría de Circuitos, Universidad Politécnica de Madrid, where he has been with the Departamento de Señales, Sistemas y Radiocomunicaciones, since 2014. In 1990, he became a Profesor Interino and, in 1992, a Profesor Titular de Universidad. His current research interests include the analysis and characterization of waveguides, transmission lines, planar structures and periodic structures, the analysis and design of microwave and millimeter-wave passive devices, numerical optimization techniques (genetic algorithms and evolution programs), and the analysis and applications of composite right–left-handed transmission lines and waveguides.

Dr. Esteban was a recipient of the Spanish Ministry of Education and Science Scholarship from 1988 to 1990.